CH-99-6-5

# A CFD Study for Cold Air Distribution Systems

**Shih-Cheng Hu, Ph.D.**
*Associate Member ASHRAE*

**John Michael Barber, C.Eng.**

**Yew Khoy Chuah, Ph.D.**
*Member ASHRAE*

## ABSTRACT

*This paper presents a computational fluid dynamics (CFD) study of the indoor environment provided by a cold air distribution system using three alternative types of diffusers, i.e., a square multi-cone type, a wall-mounted nozzle type, and a ceiling nozzle type. The surface condensation risk on the diffusers is also discussed using the CFD results and a simple condensation model. An innovative proposal to prevent surface condensation and cold air dumping when using multi-cone circular diffusers with cold air is presented. The results show no significant variation in temperature distribution, airflow patterns, mean age of air, and mean carbon dioxide concentration at the occupied zone using a conventional chilled air system compared with a cold air distribution system. The ceiling nozzle type diffusers are suitable for cold air distribution systems. The wall-mounted nozzle type diffusers lose their jet momentum very fast because of reversed flow, and, therefore, they have a very limited range of cooling areas. The risk of surface condensation on the diffuser increases as the supply flow rate increases. The influence of the multi-cone diffuser lips on airflow diffusion is very significant.*

## INTRODUCTION

A cold air distribution system has been defined as a system that supplies cold air directly to rooms. The cold air has a temperature range of 4°C to 10°C, being 5°C to 10°C lower than that in the conventional chilled air supply system. In this study, the supply temperature of cold air distribution systems is 8°C, while the supply temperature of the conventional systems is 14°C. The cold air distribution system has become more popular of late. However, there are some concerns for this system including (1) possible cold air dumping in the occupied spaces resulting in local thermal discomfort, (2) increased condensation risk on the diffuser or terminal unit surfaces and ducts, (3) increased risk of local stagnation and consequent low air quality due to lower air change rates and incomplete mixing of cold air and room air, and (4) consequent buildup of static electrical charges and unacceptably low humidities when used in temperate regions due to the low moisture content of the cold air. Of the problems listed above, the cold air dumping and surface condensation are possibly the most significant. Cold air dumping can be solved by using a fan-powered mixing box (FPMB). The FPMB mixes room air with cold air before delivering it to the room. However, there are several disadvantages including the following: (1) the use of small, low-efficiency fans and motors in the FPMB offsets the fan energy savings arising from the use of cold air (20% to 40% lower than in conventional systems [Elleson 1993]); (2) the installation and maintenance of the FPMB is an additional cost to the whole system; and (3) there is a problem with noise arising from the fans of FPMB. Mixing boxes do not need to be used if the cold air can be mixed with the room air before entering the occupied zone. One solution is the use of a diffuser that is designed to induce a large amount of room air into the jet, such as a nozzle type diffuser. Currently, there are two types of nozzle diffusers available on the market, i.e., the ceiling nozzle type diffuser and the wall-mounted nozzle type diffuser. These high-induction diffusers are designed to mix primary air with a high volume of room air at the diffuser outlet. The effective supply air temperature rapidly increases to the conventional supply temperature a short distance from the diffuser. Knebel and John (1993) conducted several field tests and showed that cold air can be successfully supplied to

**Shih-Cheng Hu**, previously a Ph.D. candidate at the University of Liverpool, U.K., is currently an assistant professor and **Yew Khoy Chuah** is an associate professor in the Department of Air-Conditioning and Refrigeration, National Taipei University of Technology, Taipei, Taiwan, ROC. **John Michael Barber** is a lecturer on building services with the School of Architecture and Building Engineering, the University of Liverpool, Liverpool, U.K.

a room to produce a comfortable indoor environment under most operating conditions by using the ceiling nozzle type diffusers. However, the performance of the associated jet and field velocities and temperatures are not given. The airflow produced by wall-mounted terminal devices has been investigated by Jackman (1971) and recently by Melsem et al. (1996). However, these studies were for conventional air distribution systems, e.g., where the temperature difference between terminal outlet and room is less than 10°C. Li et al. (1994) and MacCracken (1993) gave a brief description of cold air distribution using wall-mounted nozzles. Knappmiller and Kirkpatrick (1994) and Kirkpatrick and Knappmiller (1996) used the computational fluid dynamics (CFD) technique to study the cold air jet produced by a slot diffuser and the associated indoor thermal comfort index. Kirkpatrick (1995) visualized the temperature field of diffuser outlet flow using liquid crystal sheets. Rose and Seymour (1993) provided some guidance as to the best implementation of cold air distribution with slot type diffusers using CFD analysis. Recently, Hu et al. (1998) conducted a detailed velocity, temperature, and surface condensation test for a multi-cone circular diffuser, a ceiling nozzle-type diffuser, and a ceiling vortex diffuser. The danger of surface condensation on the inner cone of the multi-cone circular diffuser was identified. In general, surface condensation will form if the surface temperature of the diffuser is lower than the dew-point temperature of ambient air next to the surfaces. This problem is also seen with ductwork if the insulation and vapor barrier are insufficient or if any cold air leakage occurs. For the surface of a diffuser, this is a problem, especially in a high initial temperature and humidity condition. This initial condition is known as hard start-up and can be seen in many circumstances. An example would be if there was an emergency weekend executive staff meeting that required a meeting room to be cooled rapidly during a weekend setback control sequence. In such a case, much condensation will be formed on the surfaces of the diffuser. The presence of surface condensation can promote growth of unhealthy and smelly mold and produce unwelcome damage of structural and/or aesthetic nature.

The performance of a multi-cone circular diffuser is difficult to analyze by experimental methods because the effective outlet area is not a constant value and depends on the flow patterns and diffuser geometry. Therefore, instead of using the direct measurement method, numerical methods are adopted. However, numerical evaluation of the room air movement by a multi-cone circular diffuser is also problematic because the computational grid in the room tends to be rectangular and, therefore, not well suited for a radial type of flow. The second difficulty is that the size of a multi-cone diffuser is usually much smaller than the room, resulting in a very large mesh aspect ratio in the location of the interface between the ceiling and the multi-cone diffuser. Therefore, simple representations of the diffuser have been adopted in previous studies, for example, Jiang et al. (1992), and Mizutani et al. (1995). However, the detailed flow information near the cone surfaces may be lost. Also, numerical simulations of surface condensation need to combine the heat, water vapor concentration, and airflow models, which results in an additional difficulty in numerical modeling. Heikkinen and Pira (1994) tested several simple representation methods to simulate the airflow in rooms using a circular ceiling diffuser. Chen (1997) indicated that a body-fitted coordinate or an unstructured grid system is more suitable than a small-step cylindrical coordinate system in the simulation of a complex air diffuser. Sakamoto et al. (1994) measured the condensation rate on a metal plate under various airstream velocities and humidities. To date, literature on improving the control of airflow diffusion and condensation on multi-cone diffusers seems sparse, so this paper aims to begin rectifying the problem. This involves a study of geometric parameters using the CFD technique.

Based on the above, the objectives of this study, therefore, are

1. to develop a CFD model that includes the influence of air humidity and surface condensation, for assessing the indoor thermal comfort,
2. to validate the CFD model with experimental data,
3. to compare the air velocity, temperature and thermal comfort levels, and ventilation performance of a cold air distribution system and a conventional system in a room with the same room heat load conditions,
4. to assess the influence of the geometry of a multi-cone diffuser on its air diffusion performance and condensation risk and propose a method to mitigate the problems of cold air dumping and surface condensation for multi-cone circular diffusers.

## MATHEMATICAL MODELS

### Airflow Model

Most airflows in buildings are turbulent. The turbulent model used in this study is the standard $k$-$\varepsilon$ turbulence model. With this eddy-viscosity turbulence model, the airflow, energy, and water vapor concentration transport can be described by the following time-averaged Navier-Stokes equations:

$$\text{div}\,(\rho \boldsymbol{V}\Phi - \Gamma_{\phi,eff}\,\text{grad}\Phi) = S_\phi \qquad (1)$$

where $\rho$ is air density (kg/m$^3$), $\Gamma_{\phi,eff}$ is the effective diffusion coefficient (N·s/m$^2$), $\boldsymbol{V}$ is the air velocity vectors (m/s), $S_\phi$ is source term of the general fluid property, and $\phi$ can be any one of $1, u, v, w, k, \varepsilon, H$, or $C$, where $u$, $v$, $w$ are velocity components in three directions (m/s), $k$ is turbulence kinetic energy (m$^2$/s$^2$), $\varepsilon$ is dissipation rate of turbulence kinetic energy (m$^2$/s$^3$), $H$ is enthalpy of moist air (J/kg), and $C$ is the mean concentration of moisture content. When $\phi = 1$, the general equation changes into the continuity equation. For a mixture of dry air and water vapor, the dry-bulb temperature (DB) is based on the enthalpy and the mean concentration of water vapor (ASHRAE 1997).

$$DB = (H - 2501)/(1.+ 1.805\ ) \quad (2)$$

The dew point of moist air is obtained from the Young equation (Glaser 1968):

$$T_{dp} = (RH)^{1/8.02} \times (DB + 109.8) - 109.8 \quad (3)$$

where RH is the relative humidity of moist air.

## Condensation Model

Surface condensation is assumed to happen when the surface temperature is lower than the dew-point temperature of the air adjacent to the surface.

The condensation rate per unit area $L_w$ (kg/m$^2$s) on a surface is defined as

$$L_w = h_w \times (C_\infty - C_w), \quad (4)$$

where $h_w$ is the mass transfer coefficient, $C_\infty$ is the moisture content of the free stream air over the diffuser surface (kg/m$^3$), which equals the product of the free stream air density and the free stream absolute air humidity. $C_w$ is the moist content at the surface of the diffuser (kg/m$^3$), which is the corresponding moist content of the surface temperature at a relative humidity of 100%.

From the heat and mass transfer analogy theory (Incropera and DeWitt 1987),

$$h_w \propto V_\infty^{0.6} \quad (5)$$

where $V_\infty$ is the free stream air velocity over the diffuser surface (m/s), i.e.,

$$L_w = \text{const.} \times (C_\infty - C_w) V_\infty^{0.6}. \quad (6)$$

The empirical constant (const.) can be obtained by measuring the relationship between mass flux and free stream velocity. The correlation of Sakamoto et al. (1994) shows

$$L_w = (9.47 \times 10^{-6}) \times V_\infty^{0.6}. \quad (7)$$

Note the velocity range of this correlation is 0.25 m/s to 5.0 m/s. For the case where room temperature equals 30°C and relative humidity equals 60%, $C_w = 0.01891$ kg/m$^3$ and $C_\infty = 0.00826$. Hence,

$$\text{const.} = 9.54 \times 10^{-3}. \quad (8)$$

That is,

$$L_w = 9.54 \times 10^{-3} \times (C_\infty - C_w) \times V_\infty^{0.6}. \quad (9)$$

A simple formula is derived by the authors to compare the model of Sakamoto using the heat and mass transfer equations (Incropera and DeWitt 1987). Following the same experimental conditions of Sakamoto, one gets $V_\infty = 1$ m/s, Re = 4460, Dab (26°C) = 2.61E-05, Dab (8°C) = 2.38E-05, Sc = $\nu$/Dab = 0.66, where Dab is the binary diffusion coefficient of gases at one atmosphere, Sc is the Schmidt number, and $\nu$ is the dynamic viscosity (m$^2$/s). Assuming turbulent flow, the local Sherwood number is obtained following the Chilton-Colburn analogy equation (Colburn 1933):

$$Sh_x = 0.0296 \mathrm{Re}^{0.8} \mathrm{Sc}^{0.33} \quad (10)$$

$Sh_x = 0.096\ (4460)^{0.88}(0.66)^{0.33} = 21.40$. It follows that $h_{wL} = Sh_x\ (\mathrm{Dab}/L) = 0.00795$ (m/s). The analytical condensation rate for the plate is then $L_{w,ana} = 8.98 \times 10^{-5}$ (kg/s). Using the same conditions yield $L_{w,sakamoto} = 9.47 \times 10^{-5}$ (kg/s). The percentage difference relative to the result of Sakamoto is $\mathrm{diff}\% = 100 \times (L_{w,sakamoto} - L_{w,ana})/ L_{w,sakamoto} = 5.19$. Note that the difference decreases for higher velocity cases but increases for lower velocity cases. For example, diff% = 2.81 for $U = 1.5$ m/s, and diff% = 17.4% for $U = 0.5$ m/s. However, this simple analysis shows that the correlation of Sakamoto is a reliable model for this present study.

## Thermal Comfort Model

Cold draft sensation is a major concern for direct cold air distribution systems. There are several thermal comfort models available. The best known one is the predicted mean vote (PMV) model and the associated percent persons dissatisfied (PPD) (ISO 1984). However, the influence of turbulence on airflow has not been taken into account in the model. Fanger et al. (1989) proposed a mathematical model of draft risk including the influence of airflow turbulence intensity. This model has been used in this study to assess the risk of thermal discomfort due to draft sensation, which is caused by dumping of cold air. In the model, the percentage of dissatisfied people due to draft, PD, is calculated from

$$\mathrm{PD} = (34 - T_r)(V - 0.05)^{0.622}(3.14 + 0.37VT_u). \quad (11)$$

For $V < 0.05$ m/s, insert $V = 0.05$ m/s; for PD > 100%, use PD = 100%. Note that the ranges of the three parameters in the above model are $0.05 < V < 0.4$, $20°\mathrm{C} < T < 26°\mathrm{C}$, and $0.0\% < T_u < 70\%$.

The air distribution performance index (ADPI) is a single-number index for evaluating air diffusion performance in cooling conditions, which has been discussed in detail by Miller and Nevins (1972). This index includes the performance characteristics of the diffuser and room dimensions (Miller 1977). Recently, the effect of airflow turbulence on ADPI has been studied by Abu-El-Hassan et al. (1996). Their results show that the ADPI values determined using the centerline data and the whole room data were approximately the same and that the airflow turbulence and room heat load conditions strongly affect the value of ADPI. Generally speaking, an ADPI value of 80% or more can be considered to be acceptable. The ADPI is the percentage of measurement points that have air speed below 0.35 m/s and effective draft temperatures between −1.5°C and +1.0°C. The effective draft temperature is defined as

$$T_{eff} = (T - T_r) - 8.0(V - 0.15). \quad (12)$$

## Local Mean Age of Air

The local mean age of air is defined as the average time for air to travel from the supply location to any point in the room. The steady-state method of Matsumoto and Kato (1992)

and Li et al. (1992) has been adopted to calculate the distribution of local mean age of air in the present study. The transport equations for the local mean age of air ($\tau$) is

$$\text{div}\,(\rho V\tau - \Gamma\,\text{grad}\tau) = 1. \qquad (13)$$

The mean age of air ($\tau$) is considered a passive quantity and, hence, does not affect airflow patterns. The boundary conditions for the solution of the equation are zero value for the mean age of air in the supply openings and zero gradient at solid walls and at exit openings. After the flow equations have been solved, the mean age of air equation can be solved with the known airflow and viscosity data. The airflow model is solved by PHOENICS code, as developed by Rosten and Spalding (1987). A separate FORTRAN program has been coded by the authors to combine the airflow model with the condensation model, the ventilation efficiency model, and the thermal comfort model.

## CASE SETUP

The case setup is in three parts:

1. a validation exercise with three cases in an environmental chamber assessed both by experimental measurement and by CFD numerical prediction, for comparison and validation purposes (cases 1 through 3),
2. CFD studies of the thermal performance provided by the same environmental chamber (cases 4 through 12, as shown in Table 1), and
3. a parametric study for a multi-cone circular diffuser (cases 13 through 17, as shown in Table 2).

A more detailed indication for the three parts is given here.

### Part 1—Validation Exercise (Case 1 through Case 3)

The operational conditions of case 1 through case 3 are the typical conditions for cold air distribution using variable-air-volume (VAV) systems with a ceiling nozzle type diffuser, as shown in Figure 1a (effective area equal to $8 \times 10^{-3}$ m$^2$). During the experiments of case 1 through case 3, the dry-bulb temperature at the outlet duct was controlled to 24°C. The moisture source acting as latent load was 1.39 kg/s·m$^2$, 2.78 kg/s·m$^2$, and 4.18 kg/s·m$^2$ for cases 1, 2, and 3, respectively. The detailed experimental methods and conditions employed can be found in the paper by Hu et al. (1998). Note that in the experimental work, the three-dimensional velocity measurements were measured by using an ultrasonic anemometer. These measured data are used to validate the CFD model.

### Part 2—Choice of CFD Simulated Cases in an Environmental Chamber (Case 1 through Case 12)

A square ceiling diffuser with an effective area of $72 \times 10^{-3}$ m$^2$ is used for case 4, case 5, and case 6, which aim to compare the air diffusion characteristics, ventilation efficiency, and contamination distribution of cold air distribution systems and conventional systems. These cases enable us to understand the differences in operational parameters between cold air supply systems and conventional systems. It is noted that cold air dumping is expected when handling cold air with a square ceiling diffuser due to its large effective area (Kirkpatrick 1995; Kirkpatrick and Knappmiller 1996). The application of a square diffuser in cold air distribution is therefore not included in this study. The goal of cases 7, 8, and 9 is to investigate the air diffusion performance of cold air distribution using a wall-mounted nozzle type diffuser and that of a

**TABLE 1**
**Cases Studied in an Environmental Chamber**

| Case | Type | $Q$ (L/s) | $T_{in}$ (°C) | Moisture Source (kg/s·m$^2$) | Total Load (W/m$^2$) | Type of Results Obtained |
|---|---|---|---|---|---|---|
| 1 | A | 23.6 (50 cfm) | 8 | 1.39e-6 | 18.9 | Meas. & pred. |
| 2 | A | 47.3 (100 cfm) | 8 | 2.78e-6 | 37.8 | Meas. & pred. |
| 3 | A | 70.8 (150 cfm) | 8 | 4.18e-6 | 56.7 | Meas. & pred. |
| 4 | B | 43.6 (92.4 cfm) | 14 | 5.83e-6 | 18.9 | Predicted |
| 5 | B | 82.5 (174.8 cfm) | 14 | 1.17e-6 | 37.8 | Predicted |
| 6 | B | 130 (277.2 cfm) | 14 | 1.75e-6 | 56.7 | Predicted |
| 7 | C | 23.6 (50 cfm) | 8 | 1.39e-6 | 18.9 | Predicted |
| 8 | C | 47.3 (100 cfm) | 8 | 2.78e-6 | 37.8 | Predicted |
| 9 | C | 70.8 (150 cfm) | 8 | 4.18e-6 | 56.7 | Predicted |
| 10 | A | 23.6 (50 cfm) | 4 | 1.39e-6 | 18.9 | Predicted |
| 11 | A | 47.3 (100 cfm) | 4 | 2.78e-6 | 37.8 | Predicted |
| 12 | A | 70.8 (150 cfm) | 4 | 4.18e-6 | 56.7 | Predicted |

Note: A = ceiling-mounted nozzle type diffuser; B = square diffuser; C = wall-mounted nozzle type diffuser.

**TABLE 2**
**Cases Studied for a Multi-Cone Circular Diffuser**

| Case | $Q$ (L/s) | $T_{in}$ | Hole Diameter | Cone Lips |
|---|---|---|---|---|
| 13 | 23.6 (50 cfm) | 8 | No hole | Yes |
| 14 | 47.3 (100 cfm) | 8 | No hole | Yes |
| 15 | 70.8 (150 cfm) | 8 | No hole | Yes |
| 16 | 70.8 (150 cfm) | 8 | 10 mm | Yes |
| 17 | 70.8 (150 cfm) | 8 | 10 mm | No |

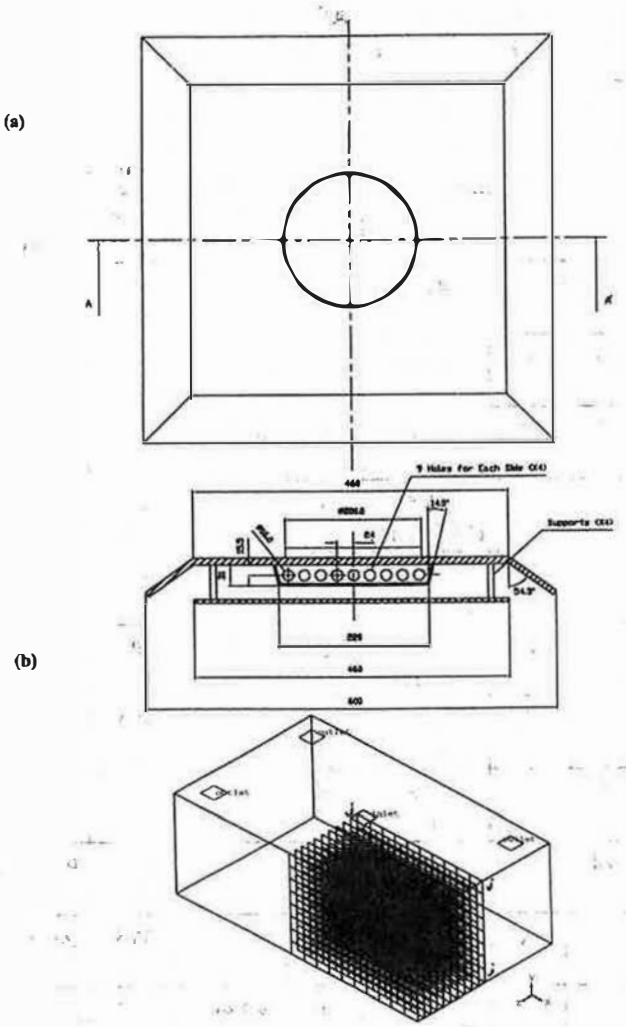


*Figure 1 (a) A four-way nozzle type diffuser; (b) volume studied. Unit: mm.*

ceiling nozzle type diffuser (cases 1 through 3). In this study, the wall-mounted nozzle type diffuser with an inclined angle of 15°, located at the level of 1.0 m from the floor, has two openings with effective areas of $1.29 \times 10^{-3}$ and $0.32 \times 10^{-3}$ $m^2$, respectively. The wall-mounted diffuser is assumed to handle a quarter volume of the environmental chamber. For case 7 and case 8, only the larger opening is used. For case 9, with a high supply flow rate, both openings are used. In order to understand the influence of supply air temperature on airflow performance and thermal comfort for the ceiling nozzle type diffuser, three cases (case 10, case 11, and case 12) have been tested with 4°C cold air. The sensible heat load and latent heat load is the same as that of case 1, case 2, and case 3.

## Part 3—Simulation for a Multi-Cone Circular Diffuser (Case 13 through Case 17)

Detailed studies of a multi-cone circular diffuser are lacking in the literature. Recently, Hirano et al. (1997) conducted a very detailed measurement of the airflow and turbulence characteristics in the outlet vicinity of a multi-cone circular diffuser using two sets of crossed hot wire anemometers. A fairly symmetrical airflow pattern was observed. Therefore, Hirano's experimental data are used to validate the present airflow model. The geometry of the multi-cone circular diffuser (with two cones) experimentally studied by Hirano et al. is shown in Figure 2a.

Table 2 summarizes the simulation cases for a multi-cone circular diffuser (with three cones, as shown in Figure 2b). Cases 13 through 15 aim to compare air diffusion characteristics of jets created by the multi-cone circular diffuser under various supply flow rates. The objective of case 16 was to determine the effect of the small hole on the risk of surface condensation on the diffuser. The purpose of case 17 was to assess the effect of the cone lip on the performance of air diffusion using a multi-cone diffuser.

## NUMERICAL METHOD AND BOUNDARY CONDITIONS

For cases 1 through 12, because of the symmetry of the airflow patters in the environmental chamber, only a quarter volume of the room was studied, as shown in Figure 1b. It is

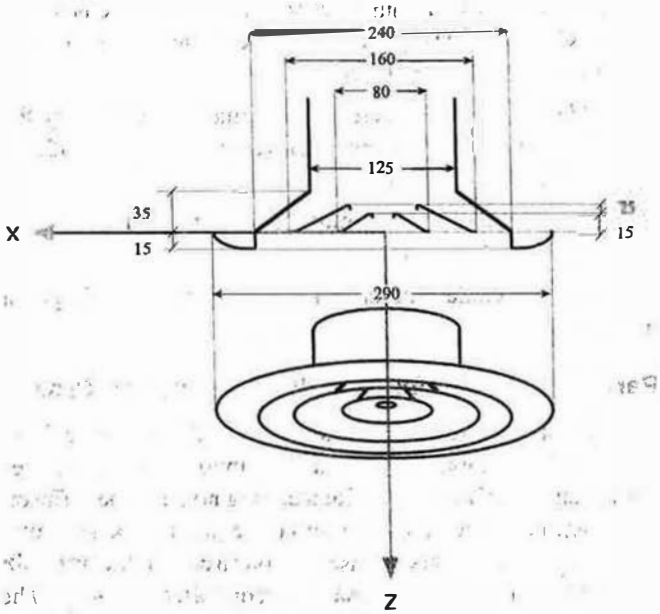


*Figure 2a The multi-cone circular diffuser measured by Hirano et al. Unit: mm.*

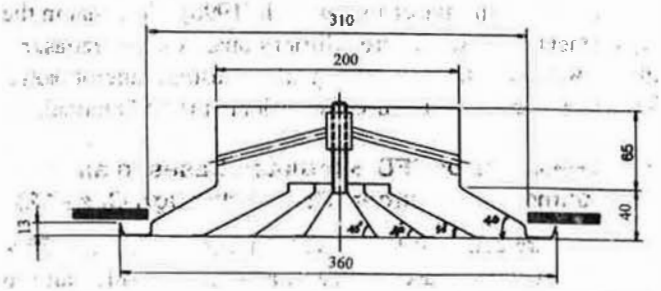


*Figure 2b The multi-cone circular diffuser studied in cases 13 through case 1. Unit: mm.*

noted that because the largest velocity, temperature, and concentration gradient occurred along the jet direction, the predicted results along the jet centerline section (section j-j in Figure 1b) are discussed. The PD in the jet centerline section is also more significant than in the whole room because this is the highest draft risk section.

The calculation domain is a quarter volume of the environmental chamber. The grid density chosen for most of the computations was $26 \times 19 \times 21$ grids alongjetwise (x), vertical (y), and transverse (z) directions, respectively. This grid density accommodated both memory size limitations and tolerable numerical diffusion. The grid test was completed by using a denser grid system ($45 \times 26 \times 42$). However, no appreciable difference was observed. Staggered control volumes were used. The finite-difference form of the time-averaged transport equations were obtained by adopting a semi-integral approach to discretize the equations over each control volume of the computational grid using a hybrid-difference scheme. The line-by-line method was used to obtain converged solutions iteratively, whereas relaxation factors and false time steps were employed to promote stability of the process. The final relaxation factor and false time step used are indicated here. The relaxation factors were 0.7, 0.3, and 0.3 for pressure, turbulence kinetic energy, and turbulence kinetic energy dissipation rate, respectively. The false time steps were $5.56 \times 10^{-4}$, $5.56 \times 10^{-4}$, $5.56 \times 10^{-4}$, $5.56 \times 10^{1}$, $5.56 \times 10^{1}$, $5.56 \times 10^{1}$, and $5.56 \times 10^{1}$ for three velocity components, enthalpy, moisture contents, concentration of carbon dioxide, and mean age of air, respectively. The turbulent viscosity field was also underrelaxed with a value of 0.3. A run was considered to be converged if the following occurred:

1. The sum of the absolute normalized residuals in each control volume for pressure was controlled to less than $10^{-3}$.
2. The values at the monitor point stopped changing.
3. The residuals reached the cutoff point or were reduced by several orders of magnitude.

The velocity field needed about 20,000 iterations to satisfy the convergence criterion, whereas the pressure, enthalpy and moisture content, mean age of air, and carbon dioxide concentration required about only 12,000 iterations. The typical real-world computation time for 20,000 iterations at a typical grid density on a PC with Pentium-Pro 200MZ CPU, 128 MB memory, is about 20 hours. Most of the computations were started with the initial condition being the closest flow situation, which had previously been computed.

For cases 13 through 17, the boundary conditions imposed were those being standard practice in numerical computations. At the outlet station, which was placed 2.2 m (11 neck diameters) downstream of the diffuser inlet plane, the flow was assumed to be fully developed and the temperature and relative humidity were assumed to be 24°C and 40%, respectively. The inlet duct diameter was assumed to be 0.2 m (8 in.) and the temperature was assumed to be 8°C. A uniform velocity profile is assumed at the inlet plane. The multi-cone circular diffuser was assumed to be circularly symmetrical to the inlet direction of the supply air; hence, only half of the section of the diffuser was studied. The body-fitted coordinate system with 'O' type grid was employed in the streamwise direction and away from the diffuser toward the room. Figure 2c shows the mesh system. Figure 2d shows the detailed diagram at the inlet region. In total, a $42 \times 23$ grid was chosen for final production runs. The iterations were terminated when all the absolute residuals (normalized by the corresponding inletp lane fluxes) were less than $5 \times 10^{-3}$. The velocity field needed about 15,000 iterations to satisfy the converge criterion, whereas the temperature and concentration required only about 9,000 iterations. The typical real-world computation time for 15,000 iterations at a typical grid density on a PC with Pentium-Pro 200MZ CPU, 128 MB memory, is about six hours.

For all cases, in the absence of turbulence measurements, uniform values for turbulence kinetic energy and its dissipation rate at the inlet boundary condition were assigned according to

$$k_i = 1.5\,(0.04\,U_i)^2 \quad \varepsilon_i = 0.1643\,k_i^{1.5}/(0.1\,d_i) \tag{14}$$

where

$k_i$ = inlet turbulence kinetic energy, $s^2/m^2$;

$\varepsilon_i$ = inlet turbulence kinetic energy dissipation rate, $s^2/m^3$;

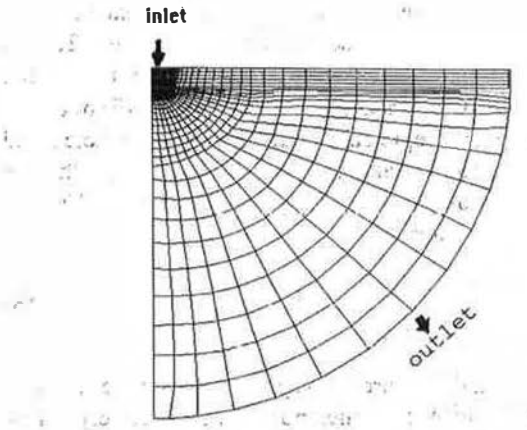


*Figure 2c The mesh system.*

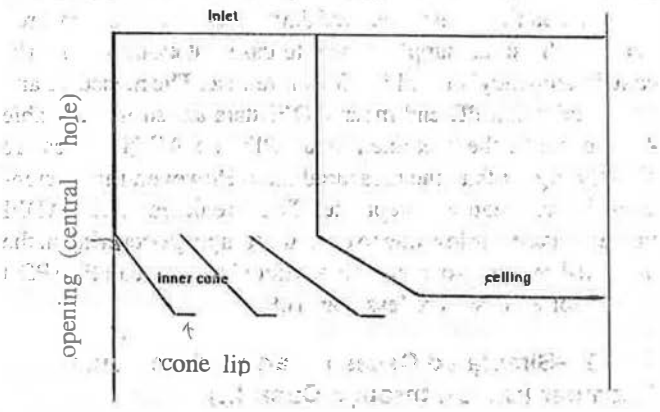


*Figure 2d The detailed diagram at the diffuser inlet region.*

$U_i$ = inlet velocity, m/s;

$di$ = inlet characteristics length, m.

## RESULTS AND DISCUSSION

### Part 1—Validation Exercise (Case 1 through Case 3)

The predicted velocity vectors of airflow for case 1, case 2, and case 3 are shown in Figure 3. For the low flow rate case (Figure 3a), the jet penetration length was approximately 2.3 m from the diffuser. Cold air dumping is observed in the occupied zone. A stagnation area formed at the upper-right region due to the lack of air circulation. For the medium supply flow rate case (Figure 3b), the jet length extended to approximately the opposite wall. There is no separation point observed for the high flow rate case (Figure 3c). The quantitative comparison for measured and predicted velocity magnitude from FL +0.5 m to +2.75 m at three stations away from the diffuser (i.e., 0.9 m, 2.1 m, and 3.3 m) for case 1 and case 3 are shown in Figures 4, 5, and 6, respectively. In general, the predicted results are in reasonable agreement with the measurements, although there are some discrepancies, especially near the ceiling region. The last measurement point is 0.05 m from the ceiling (FL +2.75 m), which is equal to the length of the sensor probe of the three-dimensional ultrasonic anemometer. This may be a possible reason for the discrepancy of some locations close to the ceiling. At the 3.3 m station, the predicted jet velocity magnitude is obviously higher than that of the measured one for cases 2 and 3.

The jet separation distance obtained from prediction, measurement, and empirical formula (Rodahl 1977) of case 1 through case 3 are depicted in Table 3. The predicted and measured throw data are also shown in this table. Note that the throw data are based on the terminal velocity of 0.3 m/s. Rodahl's empirical formula (1977) is

$$\frac{Xs}{\sqrt{A_o}} = \frac{1.81}{\sqrt{\mathrm{Ar}_o}} \tag{15}$$

where $Xs$, $A_o$, and $\mathrm{Ar}_o$ are jet separation distance, diffuser effective area, and Archimedes number, respectively. $\mathrm{Ar}_o = g\beta\sqrt{A_o}\,(T_r - T_{in})/V_{in}^2$, where $\beta$ is volumetric expansion coefficient (1/K) and $V_{in}$ is maximum jet initial velocity (m/s).

It is found that the predicted data are close to the measured ones for the small supply flow rate case but exhibit a significant discrepancy for the high flow rate case. The measured and predicted mean PD and mean ADPI data are shown in Table 4. In general, the predicted mean PD and ADPI values are slightly higher than the measured data. However, the discrepancy is reasonably acceptable. The predicted mean ADPI value for case 1 is low due to cold air dumping occurring in the occupied region. Note that the predicted room mean PD ($PD_r$) values for all cases are less than 10%.

### Part 2—Simulated Cases for an Environmental Chamber (Case 4 through Case 12)

The comparison of cold air distribution systems with conventional systems is discussed in this section. It is noted

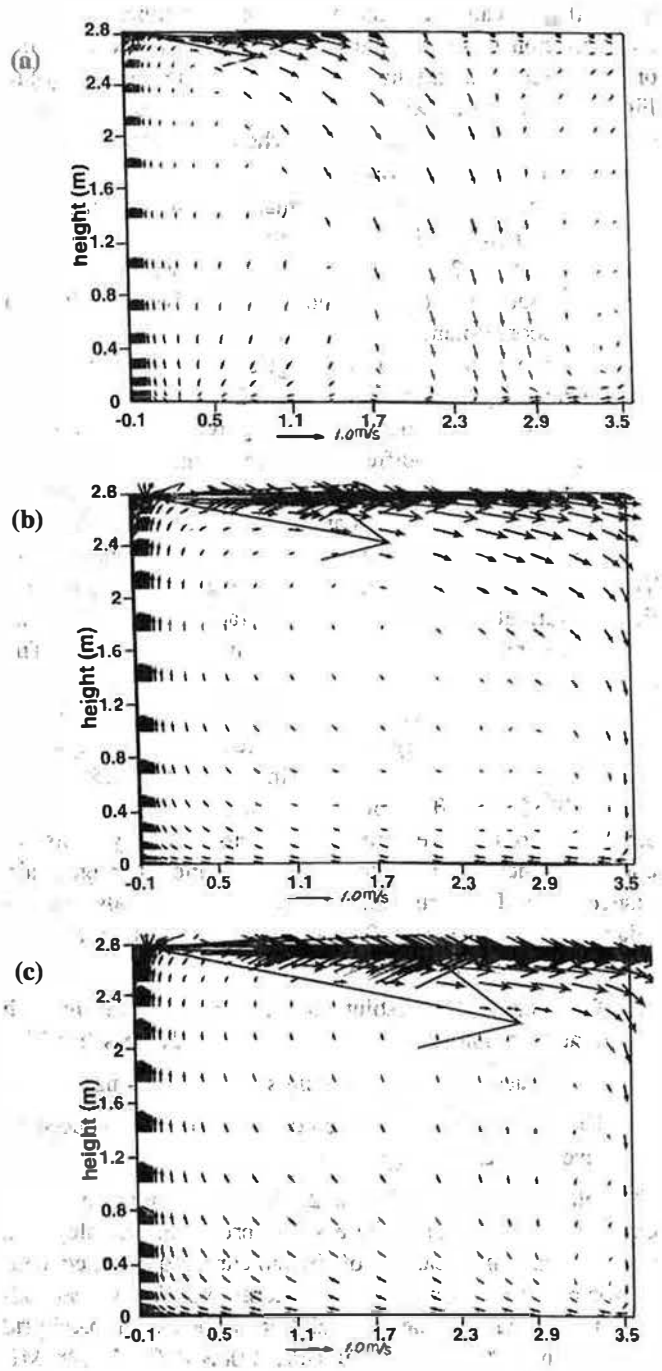


*Figure 3 Predicted airflow patterns for (a) case 1, (b) case 2, and (c) case 3. Unit: m/s.*

that there is no significant difference in airflow distribution for case 2 and case 5 (compare Figure 7a and Figure 3b), indicating the cold air distribution system produces a relatively similar airflow pattern to that of a conventional system, although the supply flow rate of a cold air system is only around half of that of a conventional system for handling the same heat load. Temperature distributions of conventional systems are quite uniform simply due to the high supply volume and the low temperature difference between room temperature and supply

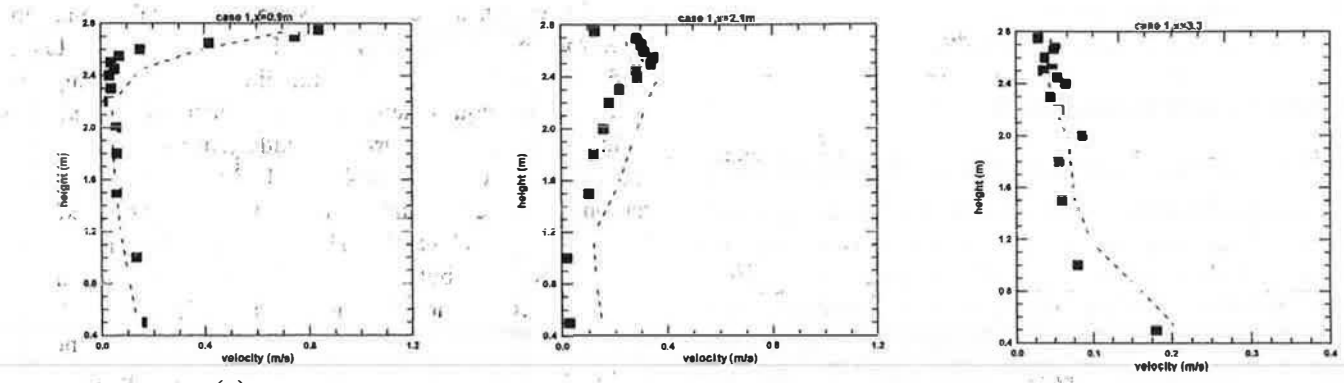


(a) (b) (c)

***Figure 4*** *Comparison between measured and predicted velocity magnitude for case 1 at stations of (a)* x = *0.9 m, (b)* x = *2.1 m, and (c)* x = *3.3 m.* ■ = *measured data,* ------- = *predicted data. Unit: m/s.*

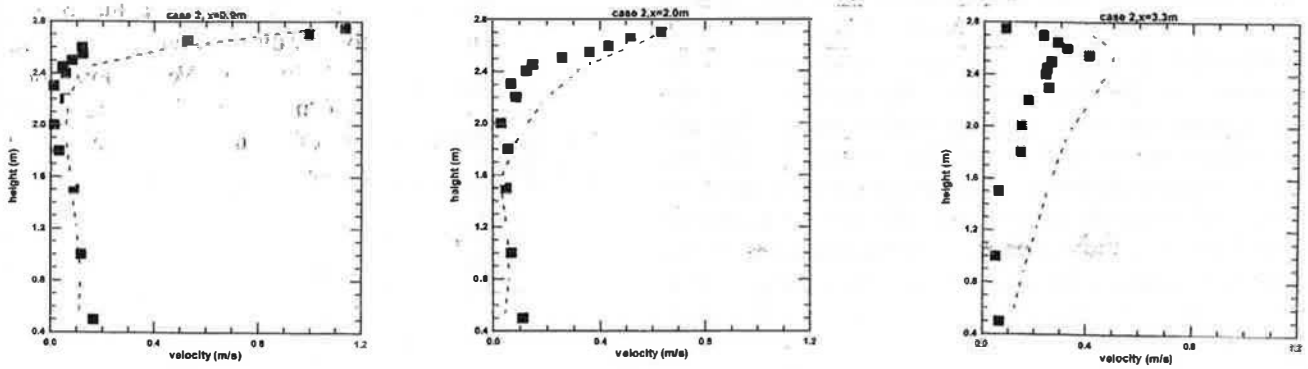


(a) (b) (c)

***Figure 5*** *Comparison between measured and predicted velocity magnitude for case 2 at stations of (a)* x = *0.9 m, (b)* x = *2.1 m, and (c)* x = *3.3 m.* ■ = *measured data,* ------- = *predicted data. Unit: m/s.*

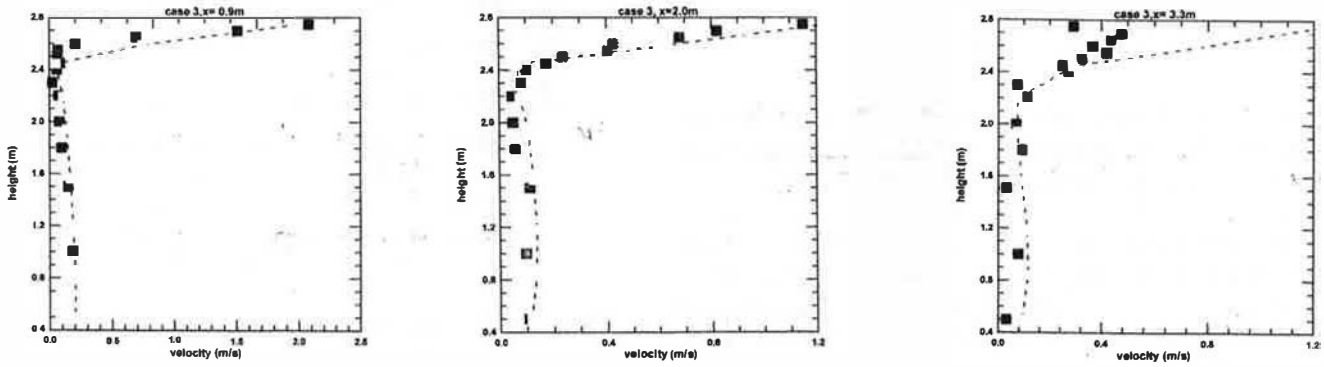


(a) (b) (c)

***Figure 6*** *Comparison between measured and predicted velocity magnitude for case 3 at stations of (a)* x = *0.9 m, (b)* x = *2.1 m, and (c)* x = *3.3 m.* ■ = *measured data,* ------- = *predicted data. Unit: m/s.*

temperature, as shown in Figure 7b. In mixing (or dilution) ventilation, where air is normally supplied outside the occupied zone, the aim of designers is to achieve a homogeneous mixing of the supply air with room air so that a uniform temperature distribution is obtained and the "contamination produced" is diluted. Cold air distribution systems using ceiling diffusers supply less volume of air than the conventional system. Consequently, most people instinctively assume a higher room contaminant concentration and a lower ventilation efficiency will be provided by a cold air distribution system. This study, however, shows that the lower supply volume of cold air distribution systems will not necessarily

**TABLE 3**
**Throw and Separation Data**

| Case | $Ar \times 1000$ | Meas. $Xs$ | Pred. $Xs$ | Empirical $Xs$ | Meas. $T_L$ | Pred. $T_L$ |
|---|---|---|---|---|---|---|
| 1 | 5.61 | 2.1 | 2.0 | 2.2 | 2.2 | 2.1 |
| 2 | 1.40 | 3.3 | 3.1 | 4.32 | 3.6 | 3.5 |
| 3 | 0.62 | NA | NA | 6.48 | NA | NA |

Note: $Xs$ = jet separation distance; $T_L$ = the throw jet; NA = not available.

**TABLE 4**
**Measured and Predicted PD and ADPI Data**

| Case | Meas. PD (%) | Meas. ADPI | Pred. PD (%) | Pred. ADPI | Pred. $PD_r$ (%) |
|---|---|---|---|---|---|
| 1 | 1.9 | 82.4 | 13.1 | 72.1 | 7.5 |
| 2 | 2.6 | 99.1 | 10.89 | 83.3 | 8.5 |
| 3 | 2.7 | 84.76 | 13.1 | 90.2 | 9.3 |

Note: $PD_r$ is the average value of PD based on the whole room data.

have this effect, as outside air supply rates will remain the same for both types of system. The volume of 20 L/s of outdoor air (about the minimum limit for two occupants' ventilation air requirements) is assumed in the simulated cases in this study. Also, the carbon dioxide generation rate of each occupant is assumed to be $4.16 \times 10^{-3}$ L/s (15 L/h), and the carbon dioxide concentration of outdoor air is assumed to be 300 ppm. Figures 8a and 8b show there is only a small variation of the distribution of carbon dioxide concentration between a conventional system and a cold air distribution system (case 1 and case 4). The figures show that if the cold air system supplies the same volume of outdoor air to the room, the room mean carbon dioxide concentration will be approximately similar to that of conventional supply air systems. However, one needs to understand that for supplying the same outdoor volume to that of conventional systems with less amount of supply air, an energy penalty at the cooling coil will result when using cold air distribution systems, reducing slightly the overall energy advantage. Ventilation efficiency can be described in term of "mean age of air." Figures 8c and 8d show the distribution of normalized mean age of air (defined as local mean age of air normalized by nominal time

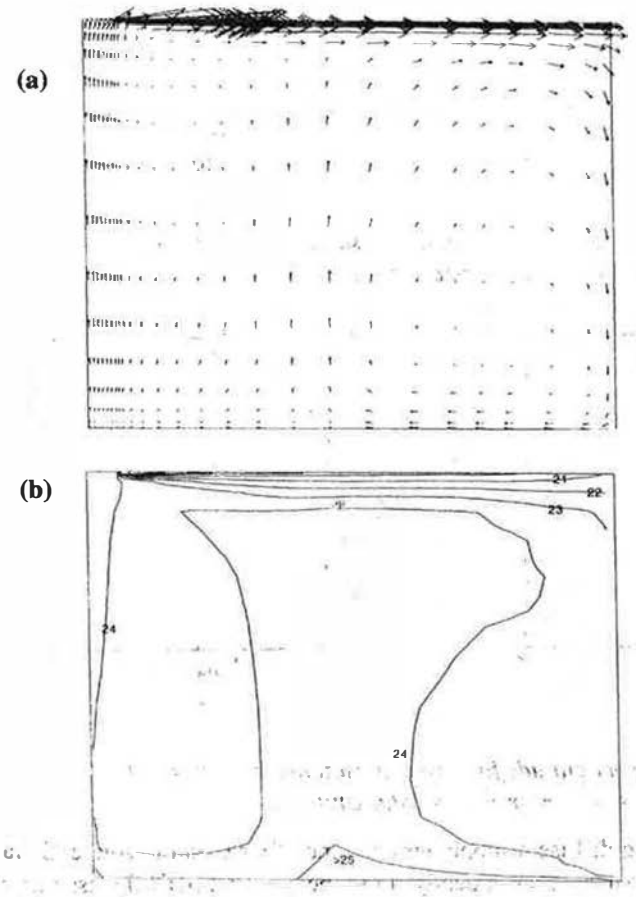


*Figure 7 (a) Velocity vectors and (b) temperature distribution for case 5.*

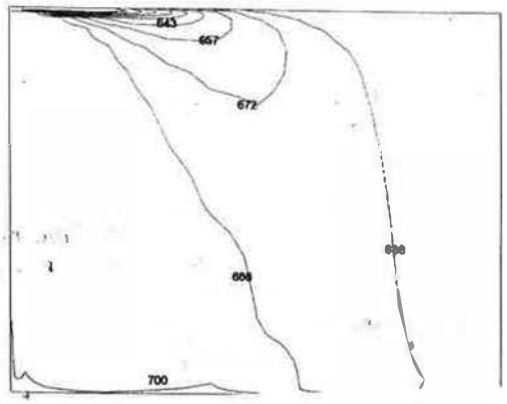


*Figure 8a Carbon dioxide distribution for case 1. Unit: ppm.*

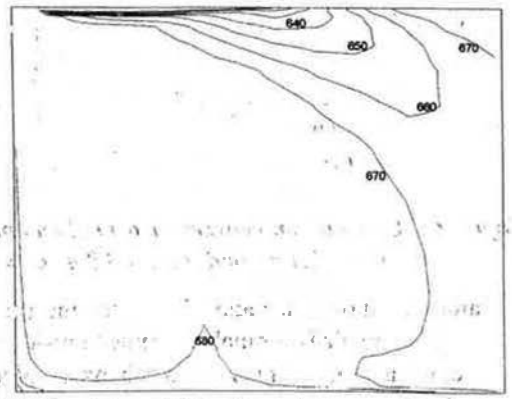


*Figure 8b Carbon dioxide distribution for case 4. Unit: ppm.*

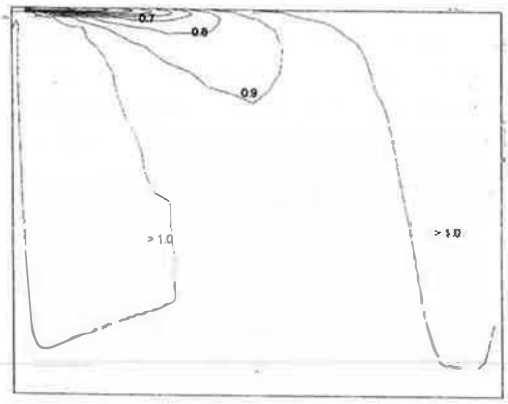


*Figure 8c Normalized mean age of air for case 1. Unit: s.*

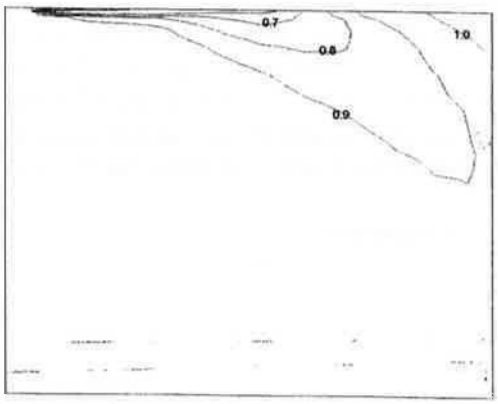


*Figure 8d Normalized mean age of air for case 4. Unit: s.*

constant, which is the ratio of room volume to the supply air flow rate). Note that the normalized mean age of air is higher in the areas under the diffuser and wall vicinities, which corresponds to the local recirculation areas that were identified from airflow patterns. It is noted that for case 1 (Figure 8c), two huge areas of the room with values of higher than unity indicates the presence of a shortcut of supply air. In general, the variation of the distribution of normalized mean age of air between the conventional system and the cold air distribution system can be considered as small. Zhang et al.'s (1994) experimental work using tracer gas shows the same characteristic. In general, the normalized mean age of air is higher in the areas under the diffuser and in wall vicinities. The locations with values greater than unity correspond to the local recirculation areas that were identified from airflow patterns. The predicted PD and ADPI values for cold air distribution systems with 4°C cold air (case 10 through case 12) and 8°C cold air (case 1 through case 3) are shown in Table 5.

It is noted that there is no appreciable difference in PD and ADPI values when directly delivering 4°C or 8°C cold air. However, the possible overdehumidifying and surface condensation of the 4°C cases should be addressed.

**TABLE 5**
**Predicted PD and ADPI Values**

| Case | Diffuser | Pred. PD (%) | Pred. ADPI (%) |
|---|---|---|---|
| 1 | Ceiling nozzle ($Ts$ = 8°C) | 13.1 | 72.1 |
| 2 | Ceiling nozzle ($Ts$ = 8°C) | 10.9 | 83.3 |
| 3 | Ceiling nozzle ($Ts$ = 8°C) | 12.1 | 90.2 |
| 7 | Wall-mounted nozzle | 6.1 | 12.5 |
| 8 | Wall-mounted nozzle | 4.8 | 67.1 |
| 9 | Wall-mounted nozzle | 7.1 | 84.5 |
| 10 | Ceiling nozzle ($Ts$ = 4°C) | 15.2 | 56.2 |
| 11 | Ceiling nozzle ($Ts$ = 4°C) | 10.7 | 78.8 |
| 12 | Ceiling nozzle ($Ts$ = 4°C) | 13.6 | 93.1 |

The flow patterns of cold air distribution using a wall-mounted nozzle type diffuser for case 7, case 8, and case 9 are shown in Figures 9a, 9b, and 9c, respectively. In general, the jet left the diffuser, traveled up, and then impinged on the ceiling. The jet behavior under the ceiling can be treated as a vertical free jet. As the jet was attached to the ceiling, it can be taken as a radial jet. It is noted that the jet of case 7 dumps soon after reaching the ceiling, while the jets of cases 8 and 9 attach and travel a short distance after impinging the ceiling. It is also found that the air velocity at the opposite side of the room is generally lower than at the diffuser side. This is due to the momentum of the impinged jet decaying fast, resulting in a significantly higher velocity in the vicinity of the jet and the ceiling. Consequently, the air velocity at the opposite side of the room is quite small. This is true for all cases tested. The throws are short; hence, this type of diffuser cannot cover a large area. Temperature distributions of cases 7, 8, and 9 are depicted in Figures 10a, 10b, and 10c, respectively. It is noted

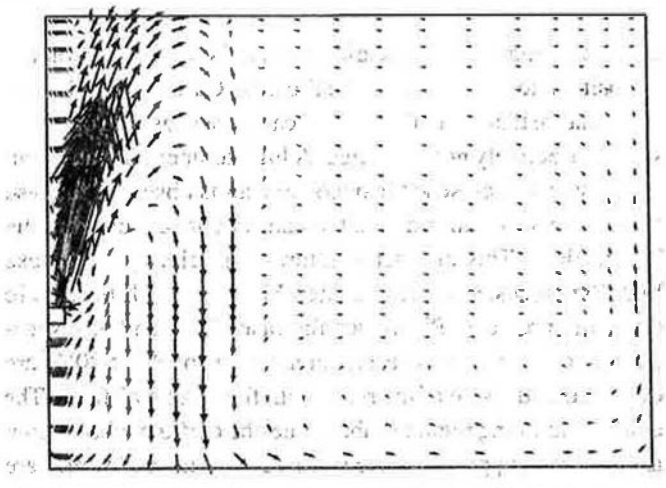


*Figure 9a Predicted velocity vectors for case 7. Unit: m/s.*

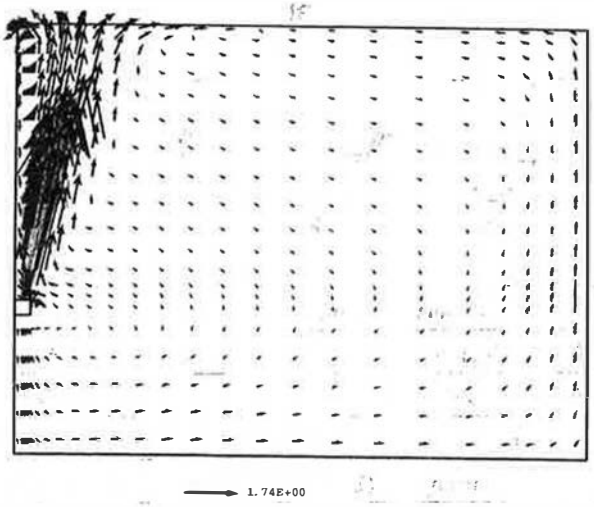


*Figure 9b Predicted velocity vectors for case 8. Unit: m/s.*

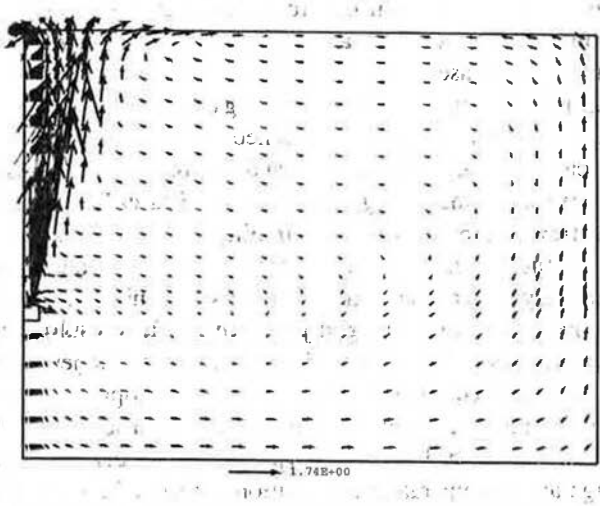


*Figure 9c Predicted velocity vectors for case 9. Unit: m/s.*

that the temperature on the diffuser side is higher than on the opposite side of the room for all cases. Case 7 has a higher temperature than that of case 8 and case 9 because the opposite side is effectively not ventilated. A high temperature and high velocity region close to the opposite wall is observed for case 8 and case 9, which is due to the natural convection from the heated floor. This high temperature and velocity will cause high PD values, as discussed later. Figures 11a, 11b, and 11c show the predicted PD values for cases 7, 8, and 9, respectively. For case 7, as expected, high values of PD (>20%) are observed at the side of the room with the nozzle diffuser. The cold air dumping region is about one-third of the whole room area. As the supply flow rate increases, the high PD areas are observed in the jet region, the floor region, and the opposite wall region. However, the occupied zones still show low PD values. The PD values are high at the floor region because of the reverse flow, which is induced by the high velocity jet. The

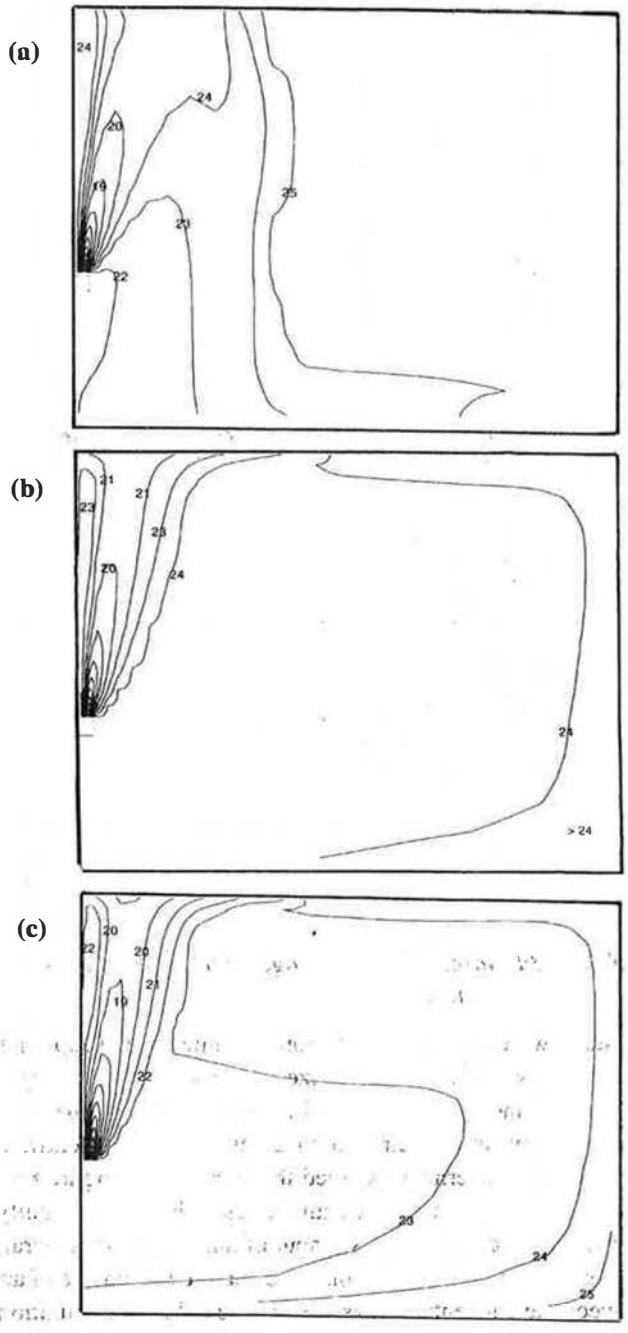


*Figure 10 Predicted temperature for (a) case 7, (b) case 8, and (c) case 9. Unit: °C.*

PD values at the opposite wall region are high because of the influence of natural convection currents from the heated floor. The PD values in this area increased as the supply flow rates increased, as seen in Figures 11b and 11c. The predicted mean ADPI values in the occupied region for case 7, case 8, and case 9 are 12.5%, 67.1%, and 84.5%, respectively, as shown in Table 5. Note that the occupied region does not include the area within 0.6 m from the diffuser. It is noted that the ADPI values increase as the supply flow rate increases. A very low

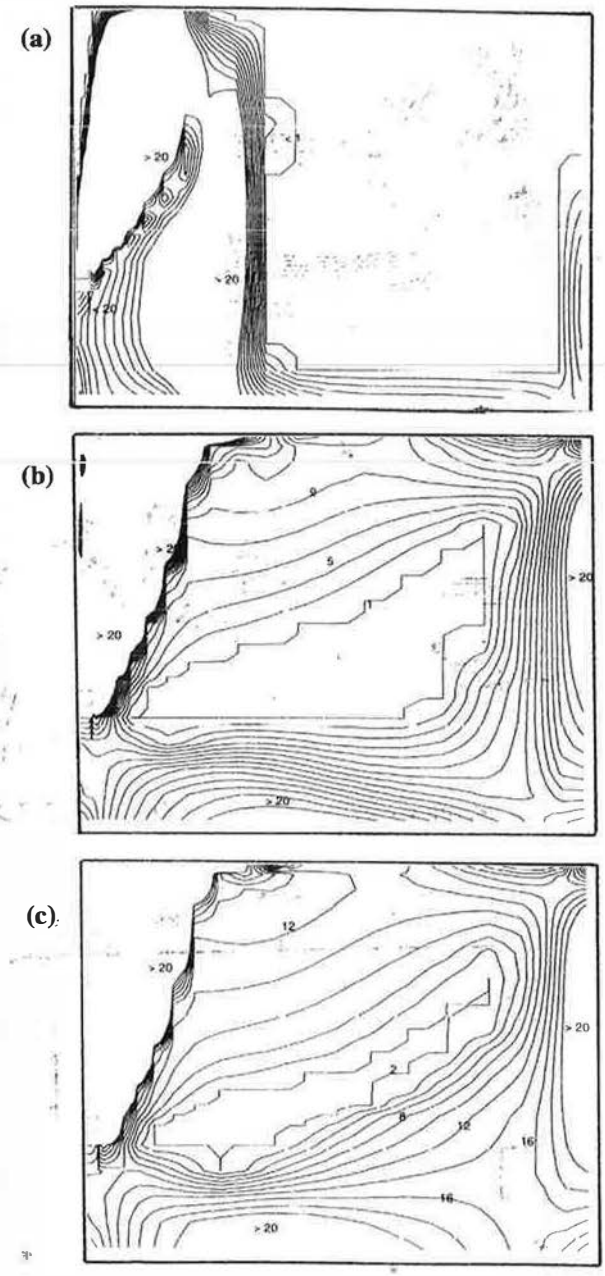


***Figure 11*** *Predicted PD distribution for (a) case 7, (b) case 8, and (c) case 9. Unit: %.*

ADPI value for the low flow rate case is because there is insufficient momentum in the jet to send the cold air to the occupied region. For the low flow rate case, most of the area of the occupied region has not been ventilated, which results in reduced cold draft sensations and a low air diffusion environment. In general, it is concluded that because the jets from the wall-mounted nozzle type diffuser lost their momentum very fast and because of reversed flow, the cold air tended to stay close to the nozzle side with the opposite side of the room always being warmer. Thermal comfort may be a problem if this type of nozzle diffuser is used to ventilate a wide room. From this study, it is recommended that high velocity and momentum at the nozzle outlets should be used to ensure an acceptable indoor thermal comfort environment.

## Part 3—Simulation for a Multi-Cone Circular Diffuser (Case 13 through Case 17)

Figures 12a and 12b show the measured and predicted velocity vectors for a validation exercise. It is noted that the volume of the predicted vortex is larger than that of the measured one. This is possibly due to the fact that the subtle effects of streamline curvature on turbulence are not included in the $k$-$\varepsilon$ turbulence model. However, the entrained airflow pattern is reproduced in the predicted velocity vectors. In general, the correlation between the predicted and measured profile of both figures is reasonably good. Figures 13a through 13e show the velocity vectors and temperature distributions for all cases studied for the multi-cone diffuser. The temperature distribution is presented in terms of the values of the difference between dew-point temperature ($T_{dp}$) air and surface temperature of cones, referred to as TDS hereafter in this paper. The cones were assumed to be made of metal with a high thermal conductivity. Therefore, the surface temperature of the cones was taken as the same temperature as the supply air (8°C). The merit of this form of presentation is that it not only shows the temperature distribution but also indicates the surface condensation risk. It should be noted that surface condensation will occur if the value of TDS is positive at that point. Note that the TDS values are positive at the surface of the inner cone for cases 13 through case 15 (the values are 0.16, 0.8, and 1.02, respectively), indicating surface condensation is likely to happen in this area. The values increase as the supply flow rate increases due to more room air being entrained toward the inner cone (see Figures 13a through 13c). The TDS values on the surfaces of the middle and the outer cones are positive because the mixing interface of room air and cold air is below the cones. Figure 13d shows the TDS distribution of case 16, which has a hole of 10 mm diameter in the middle of the center cone. Note the TDS values

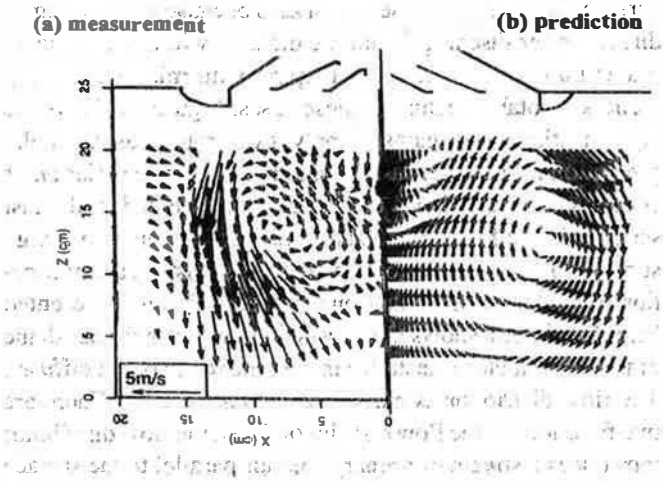


***Figure 12*** *(a) Measured and (b) predicted velocity vectors. Unit: m/s.*

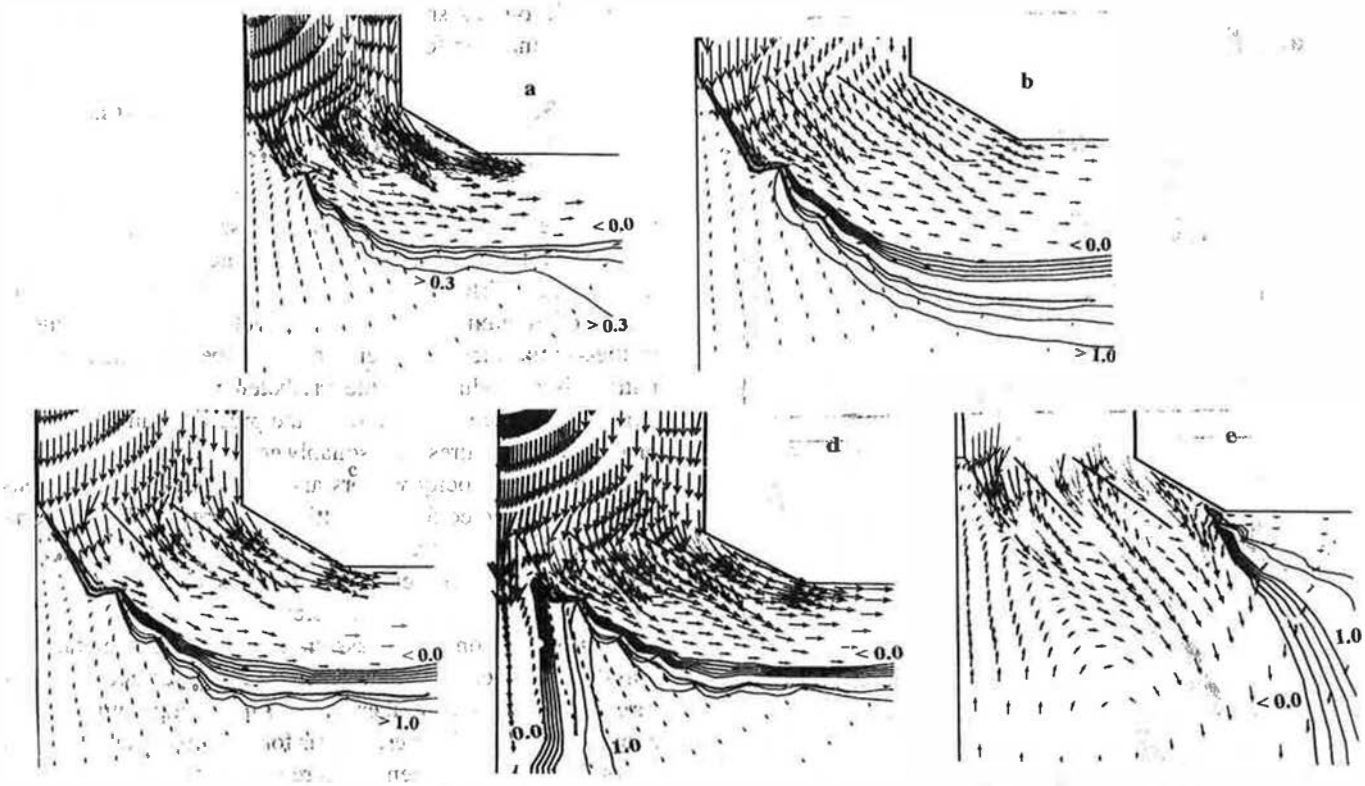


***Figure 13*** *Temperature (TDS) and velocity vectors for (a) case 13, (b) case 14, (c) case 15, (d) case 16, and (e) case 17. TDS (K) = dew-point temperature—surface temperature.*

at most of the surface of the inner cone of this case are negative except at the lower part of the cone. This is because the cold air that is introduced through the hole in the inner cone mixes with room air, thus reducing the dew-point temperature. It was also found that the TDS value at the surface of the inner cone will decrease if the diameter of the hole is increased. The manner in which the hole affects co densation is a subject for future work. However, if the hole becomes too big, there is a danger of cold air dumping. Figure 13e shows the TDS distribution at the outlet vicinity of the multi-cone diffuser that has no cone lip. It should be noted that the TDS values at all surfaces of the cones are less than zero because cold air dumps directly after discharge from the diffuser without significant induction of room air. This dumping with minimal entrainment is a notable feature of hese cases. Figure 14 shows the condensation rate against supply flow rate (based on the prediction for case 13, case 14, and case 15). The variation of condensation rate shows the same trend as noted in the last section, i.e., a high condensation rate corresponds to a high supply flow rate. Based on the above discussion, a modification proposal for the multi-cone circular diffuser is presented here. Figure 15a shows the new design, where a funnel shape of flow distributor is installed in the inner cone of the diffuser. The flow distributor is made of a porous material. There are two functions of the flow distributor. First, the flow distributor introduces a stream of primary cold air parallel to the surface of the inner cone, keeping the inner cone surface from contacting the entrained warm room air. This will prevent the inner

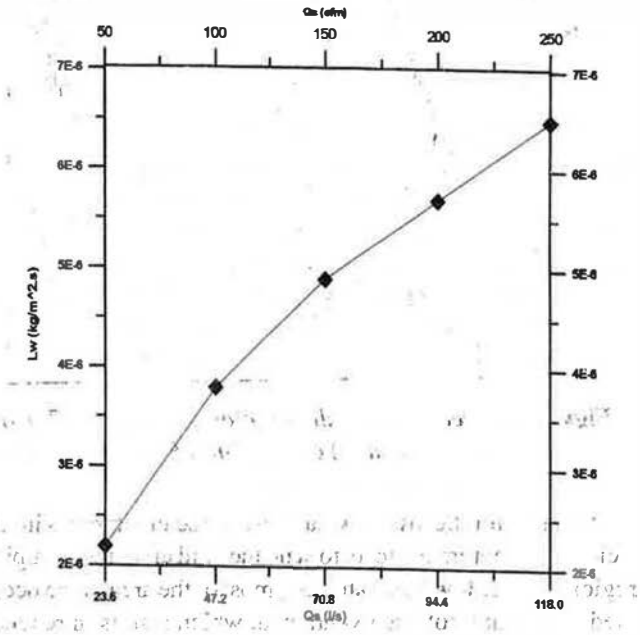


***Figure 14*** *The condensation rate (kg/m$^2$.s) against supply flow rate.*

cone surface from condensation. Second, the flow distributor reduces the speed of the downward flow, hence reducing the risk of cold draft under the diffuser. A high room temperature (26°C) and relative humidity (RH = 60%) condition is tested for the situation with and without this modification. With

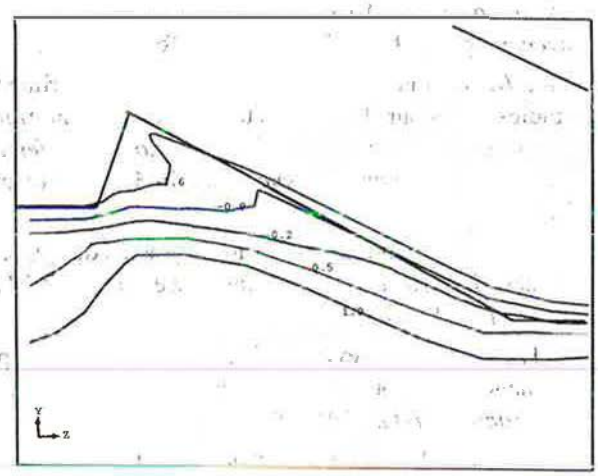

*Figure 15a CFD results for the new design diffuser. The TDS distribution for the case with modification. TDS (K) = dew-point temperature—surface temperature.*

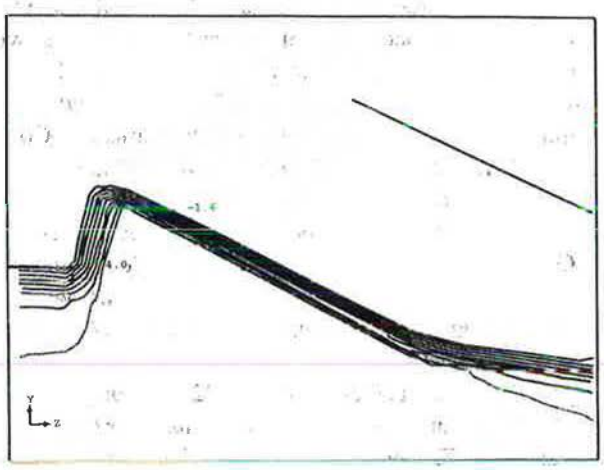

*Figure 15b CFD results for the new design diffuser. The TDS distribution for the case without modification. TDS (K) = dew-point temperature—surface temperature.*

modification (the flow distributor installed), as shown in Figure 15a, the TDS contour line at the surface of the inner cone is negative, i.e., no risk of surface condensation in the inner cone. Without modification (the flow distributor is assumed to be blocked off, i.e., porosity = zero), the TDS contour line at the surface of the inner cone is positive. In such a case, surface condensation occurs on the inner cone of the multi-cone circular diffuser.

## CONCLUSION

A CFD model for assessing indoor airflow, temperature, thermal comfort, and ventilation effectiveness using a cold air distribution system has been developed and discussed. The environmental parameters considered in this model are not only airflow patterns and temperatures but also relative humidity and surface condensation, which can be critical in cold air distribution systems. Based on the results and discussion, the following conclusions have been drawn:

- There are no significant differences in temperature distribution, airflow patterns, mean age of air, and mean carbon dioxide concentration at the occupied zone using a conventional system compared to a cold air distribution system.
- Ceiling nozzle type diffusers are suitable for cold air distribution systems. Directly supplying cold air to a room using a conventional square diffuser may result in problems of cold air dumping in occupied zones, local air stagnation, and condensation on the surfaces of the diffuser.
- Wall-mounted nozzle type diffusers loose their jet momentum very fast, and because of backward flow, the cold air tends to have a very limited horizontal penetration into the room.
- With the multi-cone circular diffuser, the risk of surface condensation increases as the supply flow rate increases. The influence of the cone lips on airflow diffusion is very significant. Modifications to the standard multi-cone circular diffuser are proposed in order to prevent the occurrence of surface condensation and cold air dumping.

## REFERENCES


Abu-El-Hassan, M.B., M.H. Hosni, and P.L. Miller. 1996. Evaluation of turbulence effect on air distribution performance index (ADPI). *ASHRAE Transactions* 102(2): 322-331.

ASHRAE. 1997. *1997 ASHRAE Handbook—Fundamentals.* Atlanta: American Society of Heating, Refrigerating and Air-Conditioning Engineers, Inc.

Chen, Q. 1997. Computational fluid dynamics for HVAC: successes and failures. *ASHRAE Transactions* 103(1): 178-187.

Colburn, A.P. 1933. *Trans. Am. Inst. Chem. Eng.* 29: 174.

Elleson, J.S. 1993. Energy use of fan-powered mixing box with cold air distribution. *ASHRAE Transactions* 99(1): 1349-1358.

Fanger, P.O., A.E. Melikov, H. Hanzawa, and J. Ring. 1989. Turbulence and draft. *ASHRAE Journal* 31: 18-23.

Glaser, H. 1968. *Kaltetechnik-Keinatisierung* 20(1): 6-11.

Heikkinen, J., and K. Pira. 1994. CFD computation of jets from circular ceiling diffuser. *Proceedings of Roomvent '94, Krakow, Poland,* Vol. 1, pp. 330-433.

Hirano, T., K. Yamanaka, T. Sato. 1997. Measurement of the airflow velocity and turbulence energy around anemostat type diffuser to verify CFD results. *Proceedings of Technical Meeting, SHASE-Japan* (B-26): 510-513 (in Japanese).

Hu, S.C., J.M. Barber, and H. Chiang. 1999. Full scale thermal performance tests of alternative diffusers when operating with cold air. *ASHRAE Transactions* 105(1).

Incropera, F.P., and D.P. DeWitt. 1987. *Fundamentals of heat and mass transfer*, 3d ed., John Wily Publishing Co.

ISO. 1984. *ISO Standard 7730-84, Moderate thermal environments—Determination of PMV and PPD indices and specification of the conditions for thermal comfort.* Geneva: International Organization for Standardization.

Jackman, P.J. 1971. Air movement in rooms with sill-mounted grilles, A design procedure. BSRIA Lab. Rep. 71.

Jiang, Z., Q. Chen, and A. Moser. 1992. Comparison of displacement and mixing diffusers. *Indoor Air* (2)168: 179.

Kirkpatrick, A.T. 1995. Visualization of diffuser outlet flow using liquid crystal sheets. *ASHRAE Journal,* August, pp. 159-164.

Kirkpatrick, A.T., and K.D. Knappmiller. 1996. The ADPI of cold air jets in an enclosure. *ASHRAE Transactions* 31(1): 3-9.

Knappmiller, K.D., and A.T. Kirkpatrick. 1994. Computational determination of the behaviour of a cold air jet in a room with a plume. *ASHRAE Transactions* 100(2): 677-684.

Knebel, D.E., and D.E. John. 1993. Cold air distribution, application, and field evaluation of a nozzle type diffuser. *ASHRAE Transactions* 99(1): 1337-1348.

Li, Y., L. Fuch, and S. Holmber. 1992. Methods for predicting air change efficiency. *Proc. of the 3rd International Conference on Air Distribution in Rooms* (2): 255-271. Aalborg, Denmark.

Li, Z., L.L. Christianson, J.S. Zhang, and A. Zhivov. 1994. Cold air jets system effects on the occupied region. *Proc. of the 4th International Conference on Air Distribution in Rooms* (2)390: 401. Krakow, Poland.

MacCracken, C.D. 1993. Cold air should be jet mixed, not distributed. *ASHRAE Transactions* 99(1): 1333-1336.

Matsumoto, H., and M. Kato. 1992. A numerical method for predicting age of air in rooms. *Proc. International Symposium on Room Air Convection and Ventilation Effectiveness*, pp. 339-344. University of Tokyo, Japan.

Melsem, A., C. Inard, and P. Barles. 1996. Experimental studies on the air flow characteristics of air-conditioned office rooms. *Proc. of the 5th International Conference on Air Distribution in Rooms* (2)387: 394. Yokohama, Japan.

Miller, P.L. 1977. Room air distribution systems design techniques: The air diffusion performance index. *ASHRAE Journal* 19(4): 37-40.

Miller, P.L., and R.G. Nevins. 1972. An analysis of the performance of room air distribution system. *ASHRAE Transactions* 78(2): 191-198.

Mizutani, K., T. Nakamura, T. Kondo, and T. Yamamoto. 1995. Numerical simulation of airflow and vent lation efficiency in a cold air delivery room—Studied of cold air delivery systems (part 4). *Proceedings of Technical Meeting, SHASE-Japan, Hiroshima* (1): 361-364 (in Japanese).

Rodahl, E. 1977. The point of separation for cold jets flowing along the ceiling. *Proc. Clima 2000, Belgrade, Yugoslavia*, pp. 219-228.

Rose, P.M., and M.J. Seymour. 1993. Use of computer modelling techniques to investigate aspects involved with cold air distribution systems. *ASHRAE Transactions* 99(1): 1366-1374.

Rosten, H.I., and D.B. Spalding. 1987. *The PHOENICS reference manual.* TR/200.

Sakamoto, T., T. Yamamoto, K. Mizutani, and T. Kondo. 1994. On the experiment of condensation on the cooled metal plates—Studies on cold air delivery systems (part 1). *Proceedings of Technical Meeting, SHASE-Japan* (D-2): 209-212 (in Japanese).

Zhang, J.S., R. Zhang, Z. Li, C.Y. Shaw, L.L. Christianson, and L.H. Sparks. 1994. An experimental study of the ventilation performance of cold air distribution systems. *ASHRAE Transactions* 100 (2): 360-367.